JCI insight

Glucocorticoids target the CXCL9/10-CXCR3 axis and confer protection against immune-mediated kidney injury

Jan-Hendrik Riedel, … , Christian F. Krebs, Ulf Panzer

JCI Insight. 2022. https://doi.org/10.1172/jci.insight.160251.

Research In-Press Preview Immunology Nephrology

Graphical abstract

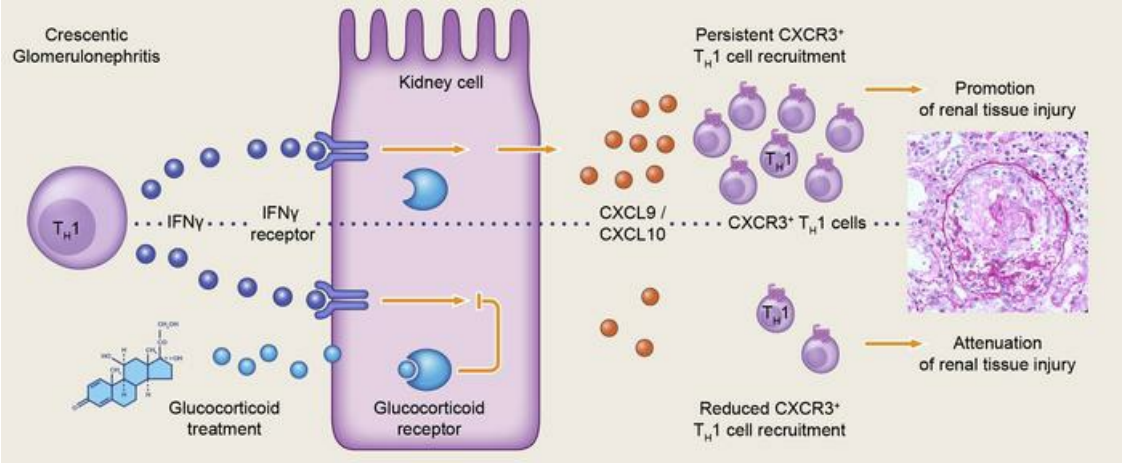

Glucocorticoids target the CXCL9/10-CXCR3 axis and confer protection against immune-mediated kidney injury

Jan-Hendrik Riedel,[1,2] Lennart Robben,[2] Hans-Joachim Paust,[1] Yu Zhao,[1,3] Nariaki Asada,[1] Ning Song,[1] Anett Peters,[1] Anna Kaffke,[1] Alina Borchers,[1] Gisa Tiegs,[4,6] Larissa Seifert,[2] Nicola M. Tomas,[2,6] Elion Hoxha,[2] Ulrich O. Wenzel,[2] Tobias B. Huber,[2,6] Thorsten Wiech,[5] Jan-Eric Turner,[2,6] Christian F. Krebs,[1,2,6] and Ulf Panzer[1,2,6]

[1] Division of Translational Immunology, III. Department of Medicine, University Medical Center Hamburg-Eppendorf, Hamburg, Germany

[2] III. Department of Medicine, University Medical Center Hamburg-Eppendorf, Hamburg, Germany

[3] Institute of Medical Systems Biology, Center for Molecular Neurobiology Hamburg, Hamburg, Germany

[4] Institute of Experimental Immunology and Hepatology, University Medical Center Hamburg-Eppendorf, Hamburg, Germany

[5] Institute of Pathology, Section of Nephropathology, University Medical Center Hamburg-Eppendorf, Hamburg, Germany

[6] Hamburg Center for Translational Immunology, University Medical Center Hamburg-Eppendorf, Hamburg, Germany

Conflict of interest: The authors declare that no conflict of interest exists.

Address correspondence to:
Ulf Panzer, M.D.
Division of Translational Immunology
III. Department of Medicine
Hamburg Center for Translational Immunology
University Medical Center Hamburg-Eppendorf
Martinistraße 52
20246 Hamburg, GERMANY
Phone: +49-40-7410-51557
Email: panzer@uke.uni-hamburg.de

Abstract

Glucocorticoids remain a cornerstone of therapeutic regimes for autoimmune and chronic inflammatory diseases, for example, in different forms of crescentic glomerulonephritis because of their rapid anti-inflammatory effects, low cost, and wide availability. Despite their routine use for decades, the underlying cellular mechanisms by which steroids exert their therapeutic effects need to be fully elucidated.

Here, we demonstrate that high-dose steroid treatment rapidly reduced the number of proinflammatory $CXCR3^+$ $CD4^+$ T cells in the kidney by combining high-dimensional single-cell and morphological analyses of kidney biopsies from patients with antineutrophil cytoplasmic antibody (ANCA)-associated crescentic glomerulonephritis. Using an experimental model of crescentic glomerulonephritis, we show that the steroid-induced decrease in renal $CD4^+$ T cells is a consequence of reduced T-cell recruitment, which is associated with an ameliorated disease course. Mechanistic *in vivo* and *in vitro* studies revealed that steroids act directly on renal tissue cells, such as tubular epithelial cells, but not on T cells, which resulted in an abolished renal expression of CXCL9 and CXCL10, as well as in the prevention of $CXCR3^+$ $CD4^+$ T-cell recruitment to the inflamed kidneys. Thus, we identified the CXCL9/10-CXCR3 axis as a previously unrecognized cellular and molecular target of glucocorticoids providing protection from immune-mediated pathology.

Graphical abstract

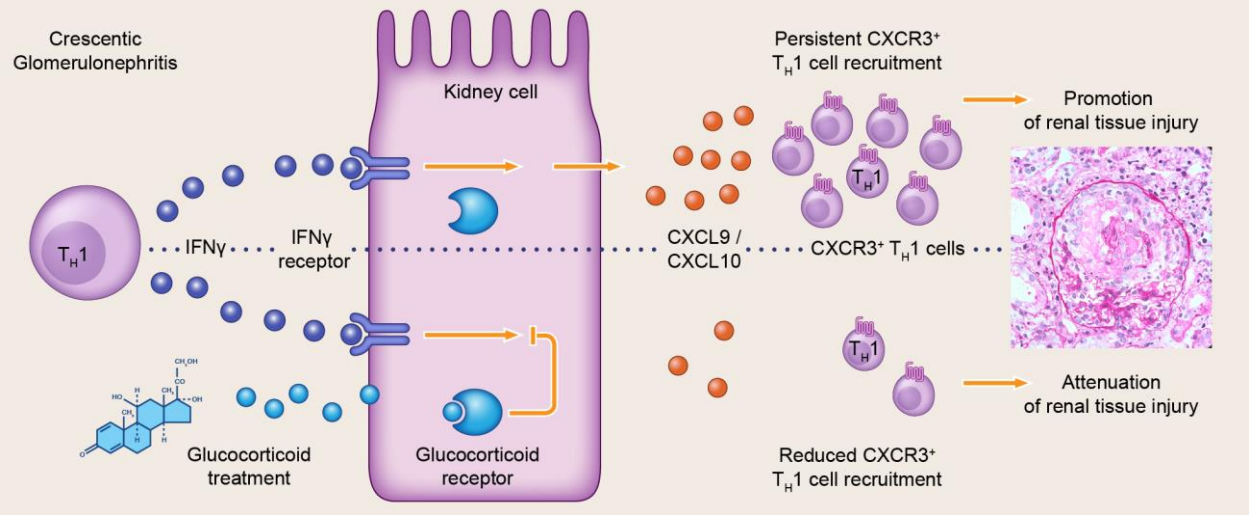

Introduction

Immune-mediated kidney diseases remain a leading cause of end-stage kidney failure worldwide. The recruitment of immune cells into the kidney is a morphological hallmark of this group of disorders that is closely correlated to the clinical outcome (1, 2). In particular, in rapidly progressive or crescentic glomerulonephritis (RPGN), infiltrating $CD4^+$ effector T cells of the T_H1 and T_H17 types release proinflammatory cytokines that directly promote tissue damage and stimulate chemokine production by renal resident cells, leading to the recruitment of additional leukocyte subsets and the subsequent loss of renal function, while the role of $CD8^+$ T cells in RPGN remains controversial (3-7).

In experiments giving rise to this study, we observed that steroid treatment markedly reduced the renal T-cell infiltrate in patients with ANCA-associated crescentic GN, the leading cause of RPGN. Further analyses revealed that particularly the number of effector $CD4^+$ T cells, not $CD8^+$ T cells, was diminished. This finding prompted our interest in investigating the underlying mechanisms of how steroids induce these therapeutic effects on $CD4^+$ T cells.

Glucocorticoids (GCs), a class of lipid-soluble, cholesterol-derived corticosteroid hormones (8), still serve as the cornerstone of frontline therapeutic regimes for autoimmune and chronic inflammatory disorders, including immune-mediated glomerular diseases, owing to their potent and rapid immunosuppressive and anti-inflammatory properties (9). The reliance on non-specific immunosuppression is often associated with severe infectious complications. Besides, the use of glucocorticoids entails a wide variety of significant adverse effects in most patients (10). GCs primarily function through binding to the cytosolic glucocorticoid receptor (GR), expressed in virtually every nucleated cell, which then translocates into the nucleus interacting with glucocorticoid-responsive elements of the DNA to activate or suppress transcription (11). However, despite their long-standing use in a wide range of inflammatory diseases, the exact mechanisms of action of GCs need to be addressed in full, both those

producing beneficial and those causing adverse effects. It is especially essential to develop new therapies with fewer adverse events.

Accumulating evidence suggests a cell type- and tissue-specific responsiveness to glucocorticoid therapy that is even more complex due to acute and chronic effects, the different types of GCs, and the dose used in clinical applications (10). Certainly, T cells are thought to be primary targets of glucocorticoid therapy. However, conflicting evidence exists concerning their responsiveness to GCs, such as cell death and proliferation, which may partially be explained by the different subtypes of T cells reacting differently to glucocorticoid exposure (8). Moreover, the effects of GCs on other leukocyte subjects, such as macrophages and neutrophils (12), and resident cells, such as epithelial cells (13), are less well characterized and may have been underrated in previous studies.

The aim of the present study was to investigate the effects of a high-dose glucocorticoid pulse regimen reflecting the standard of care for remission induction of ANCA-GN on the renal leukocyte infiltrate in human and experimental crescentic glomerulonephritis. Here, we (i) assessed the direct effects of GCs on the renal T-cell infiltrate in human and murine cGN by combining high-dimensional single-cell and morphological analyses, (ii) dissected the observed effects in terms of T-cell intrinsic vs. tissue-specific causes, and (iii) thereby identified cellular and molecule targets responsible for the glucocorticoid-mediated regulation of the renal T-cell infiltrate in human and experimental cGN.

Results

Glucocorticoid treatment rapidly reduces the renal CD4$^+$ T-cell infiltrate in human ANCA-GN. For a systematic analysis of T cells from patients with crescentic glomerulonephritis, we established a workflow designed to generate histological and single-cell data from a pool of patients with biopsy-proven ANCA-GN (Figure 1A). We were able to recruit almost equal numbers of patients with ANCA-GN who had been treated with one up to three pulses of intravenous glucocorticoids (ANCA-GN + steroids) and patients who had not been treated (ANCA-GN) before kidney biopsy but had comparable baseline characteristics (Supplemental Figure 1). Periodic Acid-Schiff (PAS) staining revealed similar levels of tissue injury in both groups (Figure 1B). Furthermore, a clinicopathological score designed to predict renal outcomes in ANCA-GN patients (14) showed a similar distribution, ruling out a selection bias towards healthier patients in the treatment-naïve group. The high-dose intravenous glucocorticoid treatment significantly reduced the number of CD3$^+$ T cells determined by semiquantitative analysis of immunohistochemical CD3$^+$ staining (Figure 1B). This was corroborated by flow cytometric data of intrarenal T cells gathered from kidney biopsy material of ANCA-GN patients. Analyses revealed CD3$^+$CD4$^+$ T cells as the main T cell subtype in the inflamed kidneys (Figure 1C) with absolute CD3$^+$CD4$^+$ T-cell numbers significantly reduced in ANCA-GN patients treated with glucocorticoids while CD3$^+$CD8$^+$ T cells were only marginally decreased (Figures 1C and 1D).

Glucocorticoids decrease the CD4$^+$ T-cell number in the kidney in an experimental model of crescentic glomerulonephritis. To make a detailed assessment of the steroid-induced changes in T-cell number and function, we aimed at studying this question in a well-established model of murine crescentic glomerulonephritis (cGN) (15). In line with protocols used in humans, cGN high-dose steroid treatment (prednisolone 7.5 mg/kg body weight at indicated time points) effectively reduced kidney injury in terms of histopathological and functional kidney damage,

and $CD3^+$ T-cell numbers were significantly decreased in parallel (Figure 2, A and B, and Supplemental Figure 2, A-C). We, furthermore, performed histological, flow cytometric, and scRNAseq analyses after a short high-dose steroid treatment regimen (Figure 2C). In this setting, immunohistochemical analyses showed that $CD3^+$ T cells were reduced (Figure 2D) as seen in the human data, while numbers of mononuclear phagocytes and neutrophils remained unchanged (Supplemental Figure 3). The $CD4^+$ T-cell subset was primarily diminished in the kidneys of steroid-treated compared to untreated nephritic mice when further analyzed by flow cytometry, while the $CD8^+$ T-cell subset was not (Figure 2, E and F). Unsupervised scRNAseq analyses of renal $CD3^+$ T cells resulted in nine different clusters in the Uniform Manifold Approximation and Projection (UMAP) space, showing an unexpected paucity of differentially expressed genes (Figure 2G and Supplemental Figure 4, A and B). However, when analyzing the cells by origin, that is, by measuring the respective fraction of sampled cells contributing to specific clusters of interest, we detected a substantial shift in $CD4^+$ T cell clusters from memory $CD4^+$ T cells towards naïve $CD4^+$ T cells. By contrast, $CD8^+$ T cells and regulatory T cells remained stable (Figure 2H). Analysis of circulating autologous mouse anti-sheep antibodies revealed similar levels of total IgG as well as IgG subclass antibodies ruling out a B cell mediated effect of glucocorticoid treatment (Supplemental Figure 5).

CD4 T-cell (pre-)apoptosis and proliferation and emigration to the draining renal lymph node (rLN) are unaffected by steroid treatment in murine cGN. Studies in malignant and in (auto-)inflammatory diseases suggest a significant effect of steroids on leukocyte survival and proliferation (16, 17). Hence, we aimed at analyzing these factors as potential contributors to the reduction in the renal T-cell infiltrate found in our model. We performed immunohistochemical and flow cytometric analyses of (pre-)apoptosis and proliferative capacity of $CD4^+$ T cells using the experimental setup described before (Supplemental Figure 6A). While the evaluation of kidney tissue slides revealed no increase in apoptotic lymphocytes,

we found a reduction in proliferating lymphocytes, which is likely to be a consequence of the overall decrease in the T-cell infiltrate (Supplemental Figure 6, B and C). Flow cytometric data corroborated these findings by showing unchanged proportions in $CD4^+$ T-cell (pre-)apoptosis and proliferation in the two nephritic groups (Supplemental Figure 6D). To rule out an augmented egress of T cells from the kidney through high-dose steroid treatment, we analyzed leukocyte numbers and proportions in the renal draining lymph node, in addition to the renal T-cell infiltrate. In steroid-treated mice, the lymph nodes contained significantly fewer total leukocytes and, while the proportion of $CD4^+$ T cells of all $CD45^+$ leukocytes remained unchanged, their total numbers were significantly reduced, likely following the decreased renal $CD4^+$ T-cell infiltrate but not causing it (Supplemental Figure 6, E and F).

Glucocorticoid receptor (GR) deficiency in T cells does not prevent the reduction in renal $CD4^+$ T cells by glucocorticoids. To test whether the decrease in renal T-cell infiltrate by high-dose steroid treatment might be caused by T-cell intrinsic factors, we induced cGN in mice deficient in the glucocorticoid receptor (GR), specifically in T cells (Lck^{Cre} x $GR^{fl/fl}$ mice), and in mice without Cre expression using the established steroid treatment approach (Figure 3A). Cre-induced excision of the GR in T cells did not lead to changes in the $CD3^+$ T-cell infiltrate measured by immunohistochemical CD3 staining (Figure 3B) or to differences in kidney damage in terms of histological and functional parameters (Figure 3, C and D). There was no change in T-cell numbers between the two groups in flow cytometric analyses of total $CD3^+$, $CD4^+$, CD8 T cells (Figure 3, E and F), or cytokine-producing $CD4^+$ T cells (Supplemental Figure 7A). The immunohistochemical FoxP3 staining performed to quantify regulatory T cells (Tregs) (Supplemental Figure 7B) did not show changes, either. Furthermore, $GR^{fl/fl}$ mice with and without Cre expression were equally susceptible to cGN induction with comparable of disease burden (Supplemental Figure 7C). Taken together, these findings argue against direct effects of steroids on T cells in cGN.

Glucocorticoid treatment changes the renal inflammatory environment to attenuate CD4$^+$ T-cell recruitment. Next, we sought to investigate whether renal T-cell recruitment could be perturbed by steroid treatment, particularly whether steroids might operate through a direct effect on target cells, or whether changes in the inflamed environment could cause the reduction in the renal T-cell infiltrate. In a first step we, therefore, transferred CD4$^+$ T cells from nephritic steroid-treated mice or nephritic untreated mice into untreated *RAG1$^{-/-}$* mice (Figure 4A). Flow cytometric analysis showed a comparable ability of CD4$^+$ T cells to migrate into the inflamed kidneys of *RAG1$^{-/-}$* recipient mice, regardless of whether these cells had been steroid sensitized or not (Figure 4B).

In a second step we transferred CD4$^+$ T cells from untreated nephritic mice into RAG1$^{-/-}$ mice previously treated with steroids or into untreated RAG1$^{-/-}$ mice (Figure 4C). In contrast to the abovementioned result, the analysis of *RAG1$^{-/-}$* recipient mice treated with steroids before the T-cell transfer revealed a distinct reduction in renal CD4$^+$ T-cell numbers compared to untreated *RAG1$^{-/-}$* recipient mice (Figure 4D), arguing for perturbed T-cell recruitment through steroid-dependent changes in the renal inflammatory environment.

The recruitment of CXCR3$^+$ T_H1 cells in murine cGN is attenuated by glucocorticoids through the dampened production of corresponding chemokines by tubular epithelial cells. After establishing a CD4$^+$ T-cell recruitment deficit as the primary reason for the reduced T-cell infiltrate in kidneys of steroid-treated animals, we assessed the chemokine receptor expression profile of renal CD4$^+$ T cells in cGN because the chemokine/chemokine receptor system is the key regulator of directional T-cell trafficking under inflammatory conditions (15, 18, 19). On day 10 of cGN, the chemokine receptor CXCR3 is highly expressed on renal CD4$^+$ T cells, followed by CCR5, and both are markers of T_H1 cells (Figure 5A and Supplemental Figure 8). This result correlates with the finding that the two main renal CD4$^+$ T-cell clusters

identified by single-cell RNA sequencing differ in their relative chemokine receptor mRNA expression in a manner allowing the assumption to be made that the predominantly occurring CXCR3-expressing memory $CD4^+$ T_H1 cells fail to infiltrate the kidney after high-dose steroid treatment (Figure 5B). Likewise, we found that interferon-gamma (IFNy)-producing $CD4^+$ T cells were predominantly reduced in kidneys of nephritic steroid-treated mice, while the numbers of IL-17-producing $CD4^+$ T cells and Tregs were unchanged (Figure 5D and Supplemental Figure 9, A and B). In addition, the corresponding T_H1-associated cytokine and chemokine mRNA levels, most importantly *Cxcl9* and *Cxcl10*, were specifically and significantly down-regulated after steroid treatment, whereas other targets such as *Il-17a* and *Ccl2* mainly remained unchanged (Figure 5E and Supplemental Figure 9C). Next, we performed *in situ* hybridization analyses (RNAscope) to localize the renal production of the CXCR3-attracting chemokines CXCL9 and CXCL10, which was primarily detectable in cells corresponding to the proximal tubular epithelium in the periglomerular and tubulointerstitial spaces (Figure 5F). In support of this finding, *in vitro* experiments showed that the co-application of steroids abolished in a dose-dependent manner the cytokine-induced production of CXCL9 and CXCL10 by proximal tubular epithelial cells (pTECs), further corroborating the role of steroids in changing the local proinflammatory environment as a means of regulating the renal T-cell infiltrate (Figure 5G and Supplemental Figure 10).

The CXCL9/10-CXCR3 axis is a potential target of glucocorticoids that provides protection from cGN. To test whether CXCR3 deficiency abrogates the steroid-dependent reduction in $CD4^+$ T-cell recruitment to the kidney in cGN, we intravenously transferred *CXCR3*$^{-/-}$ $CD4^+$ T cells into *Rag1*$^{-/-}$ mice. According to the previously used experimental setup, we then treated them with PBS or steroids two days before sacrificing them for analyses (Figure 5H). Flow cytometric analyses of renal $CD4^+$ T cells revealed comparable numbers of cells in PBS- and steroid-treated animals and similar numbers of $CD3^+$ T cells as a result of the

quantification of immunohistochemical CD3 staining of kidney sections from the groups mentioned before (Figure 5, I and J). No differences were found in kidney damage as measured by crescent formation (Supplemental Figure 11). These findings additionally underscore the importance of the CXCL9/10-CXCR3 axis as a significant factor in glucocorticoid-mediated attenuation of T-cell recruitment.

Glucocorticoid treatment alleviates the recruitment of CXCR3$^+$ T_H1 cells to the kidneys of human ANCA-GN patients. Single-cell RNA sequencing of CD3$^+$ T cells collected from patients with ANCA-GN resulted in seven clusters in the UMAP space with robust expression of *Cd4* in selected clusters (Figure 6A and Supplemental Figure 12). In detail analysis of the two main CD4$^+$ T-cell clusters revealed elevated relative expression of CXCR3, alongside CXCR4, CXCR6 and CCR6, and a reduced expression of CCR7 in pathogenic CD4$^+$ memory T cells relative to naïve CD4$^+$ T cells (Figure 6B), corresponding to the murine dataset shown in Figures 2 and 5. In line with the transcript profiling data, flow cytometric analysis of intrarenal T cells gathered from kidney biopsy material of the same patients revealed significantly reduced absolute CD4$^+$CXCR3$^+$ T-cell numbers in glucocorticoid-treated patients (Figure 6, C and D). By contrast, the percentage of CXCR3 expression of CD4$^+$ T cells was comparable (Figure 6 E). This finding was corroborated by immunohistochemical CXCR3 staining of kidney sections from patients with ANCA-GN treated with one up to three pulses of intravenous glucocorticoids (ANCA-GN + steroids) or without treatment (ANCA-GN) before kidney biopsy revealed a reduction in CXCR3-positive intrarenal cells in the treatment group (Figure 6F) In addition to it, the combination of immunofluorescence staining of CD3 with *Cxcl10* RNAscope analysis of human kidney sections showed the preferential localization of T cells to periglomerular and tubulointerstitial areas of high *Cxcl10* mRNA expression and markedly reduced *Cxcl10* signals in patients treated with intravenous glucocorticoids compared to patients without treatment before kidney biopsy (Figure 6G).

Discussion

Here, we report that glucocorticoids rapidly reduce the numbers of proinflammatory $CXCR3^+$ $CD4^+$ T_H1 cells in the kidney and subsequent renal tissue damage in human and experimental crescentic GN. Mechanistically, we demonstrate that the glucocorticoid-induced decrease in $CD4^+$ T cells in the kidney was due to reduced $CXCR3^+$ T-cell recruitment, as a specific consequence of diminished renal expression of the corresponding chemokines CXCL9 and CXCL10. Our results suggest that the CXCL9/10-CXCR3 axis is a target of glucocorticoids that provides protection against immune-mediated renal injury.

$CD4^+$ T cells are key drivers of autoimmune diseases, including crescentic GN. Many of the effects of T cells on renal damage and repair, such as local cytokine production, depend on their presence at the site of inflammation (5). Therefore, our observation that glucocorticoids diminished their numbers in the kidney of patients with ANCA-associated GN is of interest; and even if sample sizes were rather small, which increase the risk of sampling bias, we could not detect other major between-group differences. From a conceptual point of view, four different factors may determine how glucocorticoids can regulate the number of $CD4^+$ T cells in the kidney: Infiltration of T cells, proliferation of T cells, death/apoptosis of T cells, and egress of T cells out of the kidney. To investigate these different possibilities in an experimental setting, we took advantage of a well-characterized crescentic GN model in mice that is induced by the injection of nephrotoxic serum directed against the glomerular basement membrane (20, 21). This approach triggers a strong T-cell response directed against the planted antigen, which results in a $CD4^+$ T_H1/T_H17 cell-driven formation of glomerular crescents, tubulointerstitial injury, and loss of kidney function resembling some features of human crescentic GN (1).

Our studies show that high-dose glucocorticoids significantly reduce the trafficking of $CD4^+$ T cells into the inflamed kidney with little short term influence on other immune cells, incidentally pointing to an underappreciated T cell turnover, but did not affect T-cell death, proliferative capacity, or T-cell egress. Our data on T-cell death contrast with those gathered

from the thymus, where apoptosis induction, as the primary function of endogenous GCs, is well established (22-24), while it is in line with the resistance of T cells in the central nervous system (CNS) to GC-induced apoptosis and its dispensability for treatment success was found in experimental autoimmune encephalomyelitis (EAE) (25). Moreover, data on the blocking of T-cell migration to the CNS in EAE by GC treatment reflect our findings (26), which might prove to be a potentially underrated mechanism of GC treatment in different forms of autoimmune inflammatory diseases. Further support for a dominant role of GCs in preventing T-cell migration stems from a recent study in a preclinical model of stem cell transplantation, where periprocedural GC administration prevented donor T-cell accumulation in the gastrointestinal tract without evidence of influencing apoptosis and proliferation (27).

After identifying diminished recruitment as the main factor regulating the number of $CD4^+$ T cells in the kidney following high-dose GC treatment, a T-cell intrinsic GC-mediated effect was ruled out by the finding that T cell-specific deletion of the glucocorticoid receptor did not reinstall the renal T-cell infiltrate. This finding contrasts with data published for EAE. In this model, the involvement of the GR in T cells is vital for the protection from autoimmunity (28).

Mechanistically, we show that in vitro GCs act directly on proximal tubular epithelial cells (pTECs), thereby repressing the expression of the CXCR3-corresponding ligands CXCL9 and CXCL10. Furthermore, although in vivo experiments using mice with pTEC-specific deletion of the GC receptor were so far not feasible, the combination of immunofluorescence staining and FISH not only revealed pTECs as a major source of CXCL9 and CXCL10 but also showed markedly reduced CXCL9 and CXCL10 expression of pTECs in kidney sections from GC treated mice. The chemokine receptor CXCR3 is rapidly induced on naïve T cells after activation and is highly expressed on T_H1 effector $CD4^+$ T cells, playing an essential role in T-cell trafficking and function (29, 30). Our finding that glucocorticoids predominantly acted on resident kidney cells, while a deficiency in the glucocorticoid receptor on immune cells, in this case specifically in T cells, played no role, corresponds to a recent study showing direct effects

of glucocorticoids on activated glomerular parietal epithelial cells in experimental crescentic glomerulonephritis (31). Of note, a therapeutic option to modulate parenchymal renal cells, e.g. pTECs, with the aim of generating an anti-inflammatory microenvironment in renal autoimmune diseases has recently been proposed (32) and multiple studies underscore the central role of the CXCL9/10-CXCR3 axis in the development of human and experimental immune-mediated kidney diseases, including ANCA-GN and lupus nephritis, by directing pathogenic effector T cells to the sites of inflammation, thus identifying this pathway as a promising therapeutic target (15, 18, 33-35).

The CXCR3-corresponding ligands CXCL9 and CXCL10 are secreted from cultured tubular cells stimulated with IFNγ and their production was inhibited by GCs in a dose-dependent manner, indicating a direct inhibitory effect on intracellular signaling pathways. Therefore, GCs can block the proinflammatory amplification loop of the CXCL9/10-CXCR3 axis, which is mediated by tissue-invading IFNγ-producing $CXCR3^+$ T_H1 cells and the IFNγ-induced CXCR3 ligands. This may be all the more important, as autoimmune diseases, including autoimmune kidney diseases, constitute a spectrum of disorders which exhibit activity of diverse pathogenic cytokine patterns and involvement of distinct immune cell subtypes. Systemic Lupus Erythematodes (SLE), for instance, is characterized by a prominent type I interferon signature which correlates with disease activity (36), and a high-dose glucocorticoid treatment effectively controls disease flares and activity (37, 38). Our results corroborate the notion that high dose glucocorticoids exhibit their diverging potency in autoimmune diseases by preferentially targeting particular prone cytokine pathways and leukocyte subsets (39), notably T_H1/IFNy driven disorders. Intriguingly, a recent study identified the expansion of neutrophils, called IFN^{active} neutrophils, with a distinct interferon signaling signature as the main target of beneficial glucocorticoid treatment effects in Coronavirus Disease 2019 (COVID-19) patients, which may also stem from GCs selectively targeting the T_H1/IFNy pathogenic cytokine pathway (40).

In conclusion, we identified the CXCL9/10-CXCR3 pathway as a previously unknown specific mechanism by which glucocorticoids promote their therapeutic effects in experimental and human crescentic glomerulonephritis. A better understanding of the precise targets of GCs based on their modes of action is fundamental to the development of new treatment strategies with fewer severe side effects in autoimmune and chronic inflammatory diseases.

Methods

Animal experiments. $GR^{fl/fl}$ mice and Lck^{Cre} x $GR^{fl/fl}$ mice were kindly provided by M. Friese (Center for Molecular Neurobiology Hamburg (ZMNH), Hamburg, Germany). CD45.1 mice and $RAG1^{-/-}$ mice were purchased from The Jackson Laboratory (Bar Harbor, ME, USA). $Cxcr3^{-/-}$ mice were generated by our group and bred at the animal facility of the University Medical Center Hamburg-Eppendorf. All mice were on the C57BL/6J background, and knockout mice underwent embryo transfer to meet the general standards of our institution. Age-matched C57BL/6J wildtype controls were also bred in our animal facility, and all animals were raised in specific pathogen-free conditions. In intervention experiments, the mice received either 7.5 mg/kg body weight prednisolone (MIBE GmbH Arzneimittel, Brehna, Germany) in 150 µl sterile PBS at room temperature (dosage based on those used in human ANCA-GN patients), or just 150 µl sterile PBS at room temperature via the lateral tail vein for two or seven consecutive days, depending on the experimental setup. All animal experiments were performed according to national and institutional animal care and ethical guidelines and were approved by the local committees.

Induction of experimental GN and functional studies. Nephrotoxic nephritis was induced by intraperitoneal injection of 2.5 mg of nephrotoxic sheep serum per gram of body weight into 8-12-week-old male mice as previously described (15). For urine sample collection, mice were housed in metabolic cages for 5 hours. Urinary albumin excretion was determined by standard ELISA analysis (Mice-Albumin Kit, Bethyl Laboratories, Montgomery, TX, USA), while urinary creatinine, BUN, and serum creatinine were measured using standard laboratory methods.

Real-time RT-PCR analyses. Total RNA from the renal cortex was isolated with the NucleoSpin Kit (Macharey-Nagel, Düren, Germany) in accordance with the manufacturer's

protocol. RNA was reverse transcribed with the High-Capacity cDNA Reverse Transcription Kit (Thermo Fisher, Waltham, MA). Real-time qPCR of different chemokines was performed using specific primers, and IFNy was determined with TaqMan PCR (Mm01168134, Life Technologies, Carlsbad, CA). Measurement was performed on a StepOnePlus Real-Time PCR system (Thermo Fisher, Waltham, MA) as previously described, with the 18S rRNA as a housekeeping gene and all samples run in duplicate.

Morphological analyses of murine and human tissues. In murine tissue, glomerular injury and crescent formation, deposition of PAS-positive material, and tubulointerstitial injury were assessed as described (41). In brief, paraffin-embedded sections (2 µm) were stained with antibodies directed against CD3 (A0452, Dako, Glostrup, Denmark), FoxP3 (FJK-16s, eBioscience, San Diego, CA, USA), F4/80 (BM8; Dianova BMA, Augst, Switzerland), Gr-1 (NIMP-R14; Hycult Biotech, Uden, The Netherlands), Ki67 (D3B5, Cell Signaling, Danvers, MA, USA), cleaved caspase 3 (cC3) (Asp175; Cell Signaling Technology, Danvers, MA, USA), and OAT1 (OAT11-A; Alpha Diagnostics International, San Antonio, Texas, USA). Tubulointerstitial $CD3^+$ cells in 30 high-power fields (magnification ×400) per kidney, tubulointerstitial $FoxP3^+$ cells in 30 high-power fields (magnification ×400) per kidney, tubulointerstitial $F4/80^+$ cells in 30 high-power fields (magnification ×400), tubulointerstitial $GR\text{-}1^+$ cells in 20 low-power fields (magnification ×200), tubulointerstitial $Ki\text{-}67^+$ cells in 30 high-power fields (magnification ×400) per kidney, and tubulointerstitial $cC3^+$ cells in 30 high-power fields (magnification ×400) per kidney were counted in a blinded manner. In human kidney tissue, the histopathologic kidney injury was assessed by a nephropathologist according to standardized algorithms, and the Renal Risk Score was assessed as described (14). For immunohistochemical analysis, human paraffin-embedded kidney sections (2 µm) from renal biopsies obtained from ANCA-GN patients were stained with an antibody directed against CD3 (A0452, Dako, Glostrup, Denmark) and CXCR3 (1C6; BD Biosciences, San Jose, CA, USA).

Renal $CD3^+$ and $CXCR3^+$ cells in 20 high-power fields per renal biopsy (magnification ×400) were counted. For immunofluorescence staining of CD3 human paraffin-embedded kidney sections (2 μm) from patients with ANCA-GN were stained with an antibody directed against CD3 (DAKO, A0452) after dewaxing and antigen retrieval (pH 6 for 15 minutes). All slides were evaluated using an Axioskop light microscope (Zeiss, Jena, Germany) and photographed with an Axiocam HRc (Zeiss) or by confocal microscopy with an LSM800 meta microscope (Zeiss) using the LSM software (Zeiss).

RNAscope (mRNA FISH). *Cxcl9* and *Cxcl10* mRNA detection in mice kidney sections and *Cxcl10* mRNA detection in human kidney sections were manually carried out using the RNAscope Multiplex Fluorescent Assay (Advanced Cell Diagnostics, Newark, CA, USA) according to the manufacturer's instructions. Briefly, 2-4μm formalin-fixed, paraffin-embedded (FFPE) slides were baked at 60°C for 1 hour, de-paraffinized twice in xylene for 5 minutes each, and incubated twice in 100% ethanol for 2 minutes each. The sections were then air dried and treated with RNAscope hydrogen peroxide solution (Cat. No. 322381, Advanced Cell Diagnostics) for 10 minutes at room temperature and washed with distilled water. Subsequently, they were incubated with target retrieval reagent (Cat. No.322000, Advanced Cell Diagnostics) at a boiling temperature using BRAUN food steamer (FS3000, BRAUN, Neu-Isenburg, Germany) for 15 minutes, and then washed with distilled water. A hydrophobic barrier was drawn around the sections using an ImmEdge Hydrophobic Barrier Pen (Cat. No. H-4000, Vector Laboratories, Burlingame, CA, USA). The sections were then treated with protease plus reagents at 40°C (Cat. No.322381, Advanced Cell Diagnostics) for 30 minutes and incubated at 40°C for 2 hours using probes mixed with Mm-Cxcl9-C2 probe (489341-C2, Advanced Cell Diagnostics) and Cxcl10-C3 probe (408921-C3, Advanced Cell Diagnostics) or Hs-CXCL10-C2 (311851-C2, Advanced Cell Diagnostics) diluted at a 50:1 ratio. The slides were repeatedly washed with wash buffer reagent (Cat. No.310091, Advanced Cell

Diagnostics) after each amplification step by RNAscope Multiplex Fluorescent Detection Reagent (Cat. No.323110, Advanced Cell Diagnostics). All slides were imaged using a Zeiss LSM800 confocal microscope.

Cell isolation, stimulation, and transfer in mice. Previously described methods for leukocyte isolation from murine kidneys and spleens were used (41). Cell viability was assessed by trypan blue staining before stimulation, flow cytometry, and cell transfer experiments. For stimulation, after generation of a single-cell suspension as mentioned above, isolated renal leukocytes were activated by incubation at 37°C and 5% CO_2 for 4.5h with PMA (5 ng/ml; Sigma) and ionomycin (1 µg/ml; Merck Millipore, Darmstadt, Germany) in RPMI 1640 (Gibco, Grand Island, NY) with 10% FCS. After 30 min of incubation, Brefeldin A (10 µg/ml; Sigma) was added. For $CD4^+$ T-cell transfer experiments, $CD4^+$ T cells were isolated from the respective C57BL/6J wildtype, CD45.2, and *Cxcr3*$^{-/-}$ mice using a magnetic cell separation (MACS) $CD4^+$ T-cell isolation kit (Miltenyi Biotec, Bergisch Gladbach, Germany) according to the manufacturer's instruction. Viable cells were counted using trypan blue staining, and $2x10^6$ live cells were intravenously injected into RAG1$^{-/-}$ mice 9 days after or 1 day before induction of cGN.

Human studies including isolation and flow cytometric analyses of human leukocytes. Kidney biopsies for immunopathologic analyses, flow cytometry, and scRNA-seq were obtained according to standardized operating procedures from patients with (suspected) ANCA-associated glomerulonephritis and subsequent morphological and clinical parameters were analyzed after inclusion into the Hamburg Glomerulonephritis Registry. Kidney biopsy cores meant for obtaining single cell suspensions were instantly processed by enzymatic digestion in RPMI 1640 medium with collagenase D at 0.4 mg/ml (Roche, Mannheim, Germany) and DNase I (10 µg/ml, Sigma-Aldrich, Saint Louis, MO) at 37° C for 30 minutes followed by

dissociation with gentleMACS (Miltenyi Biotec). Samples were filtered through a 30 μm filter (Partec, Görlitz, Germany) before antibody staining and flow cytometry. In each case every single cell suspension generated from individual kidney biopsy cores was measured in its entirety.

Flow cytometry and fluorescence-activated cell sorting. Measurements were performed on a BD FACS LSR II (BD Biosciences, San Jose, CA, USA), while FACS sorting was performed on a FACS AriaFusion or AriaIIIu (BD Biosciences, San Jose, CA, USA). The data were analyzed using the FlowJo software (Tree Star, Oregon, CA, USA). To minimize unspecific antibody binding, cells were either incubated with normal mouse serum (Thermo Fisher Scientific, Waltham, MA, USA) or with Human BD FC Block (BD Biosciences, San Jose, CA, USA) before staining for 10 minutes. Murine cells were stained with fluorochrome-labeled antibodies against CD45, CD3, CD4, CD8, CCR5, CCR6, CCR7, CXCR3, γδTCR, NK1.1, IL-17A, IFNγ, CD11b, F4/80 and Ly6G (Biolegend, San Diego, CA, USA; BD Biosciences, San Jose, CA, USA; eBioscience, San Diego, CA, USA; R&D Systems, Minneapolis, MN, USA), and human cells were stained with fluorochrome-labeled antibodies against CD45, CD3, CD4, CD8, γδTCR, and CXCR3 (Biolegend, San Diego, CA, USA; BD Biosciences, San Jose, CA, USA; eBioscience, San Diego, CA, USA; R&D Systems, Minneapolis, MN, USA), as previously described (42). LIVE/DEAD staining (Near-infrared, Invitrogen Molecular Probes, Eugene, OR, USA) was used to exclude dead cells during flow cytometry and to ensure cell viability after the stimulation procedure. For intracellular staining, samples were processed using Cytofix/Cytoperm (BD Biosciences, San Jose, CA, USA) according to the manufacturer's instructions.

Single-cell RNA sequencing of renal $CD3^+$ T cells. scRNAseq was performed using the 10X Chromium Controller (10X Genomics, Pleasanton, CA, USA) and single-cell libraries

were generated with the 10X Genomics Chromium Single Cell 5′v1.1 reagents kit according to the manufacturer's instructions. Fifty-nanometer cDNA was used for gene expression library construction. Quality control (QC) was performed with hsDNA Qubit (Thermo Fisher Scientific, Waltham, MA, USA) and BioAnalyzer (Agilent). The libraries were sequenced on an Illumina NovaSeq 6000 system (S4 flow cell) with 150 base pairs and paired-end configurations.

Preprocessing and quality control (QC) of scRNAseq data. 10x Genomics raw sequencing data were processed using CellRanger software (version 3.0.2, 10x Genomics, Pleasanton, CA). For the mouse data, the 10x Genomics mouse genome mm10-3.0.0 release was used as the reference genome (function cellranger count). For the patient data, the human reference genome hg19-1.2.0 was used. The matrices of cells and the unique molecular identifier (UMI) count were obtained and further processed with the R package Seurat (version 4.0.4) (43). For QC of the mouse data, we first filtered out cells in which fewer than 200 genes were detectable. To remove potential doublets, cells with more than 5,000 expressed genes (nFeature) were excluded. We removed low-quality cells with more than 2.5% mitochondrial genes among all detected genes. For the patient data, the overall number of genes detected in each cell is less than the mouse data. We kept the cells with 200-3000 genes detectable and with less than 10% mitochondrial genes among all genes.

Dimensionality reduction and clustering. The Seurat R package (version 4.0.4) was used to perform unsupervised clustering analysis on scRNAseq data. Gene counts for cells that passed QC were normalized by library size and log-transformed (function NormalizeData, normalization.method = "LogNormalize", scale.factor = 10,000). Then, highly variable genes were detected (function FindVariableFeatures, selection.method = "vst", nfeatures = 2,000). To reduce batch effects, we applied the "anchor" integration method (functions

FindIntegrationAnchors and IntegrateData, dims = 1:30) (44). The integrated matrix was then scaled with the ScaleData function (default parameters). PCA was performed on the scaled data (function RunPCA) to reduce dimensionality. 30 principal components were selected for clustering based the elbow of a PCA scree plot. The selected principal components were then used to compute the KNN graph based on the Euclidean distance (function FindNeighbors). Cell clusters were subsequently generated using the function FindClusters. The resolution parameters of the FindClusters function for the mouse and human dataset were set to be 0.15 and 0.3 respectively, determined by exploration of the top marker genes of each cluster. Uniform Manifold Approximation and Projection (UMAP) was used to visualize the clustering results. The top differential expressed genes in each cluster were found using the FindAllMarkers function (min.pct = 0.25, logfc.threshold = 0.5) with Wilcoxon rank-sum tests. The most highly expressed genes were then used to determine the cell type of each cluster. The clusters with low CD3 gene counts were removed for downstream interpretation.

Differential gene expression analysis. The Seurat FindMarker function (Wilcoxon rank-sum test) was used to perform differential gene expression analysis for each cell type between the control and steroid groups in the mouse dataset.

Data and materials availability. The raw and processed sequencing data are deposited at Gene Expression Omnibus (GEO) repository under accession number GSE 217508.

Culture and stimulation of mouse kidney tubular cells. Mouse kidney tubular cells (45) were cultured in DMEM (Life Technologies, Karlsruhe, Germany) containing 3-10% FCS (Gibco), 100 U/ml penicillin, and 100 µg/ml streptomycin (Life Technologies) at 37 °C with 5% CO_2. Before stimulation, confluent cells were incubated in serum-free DMEM for 24 h. Cells were stimulated with either 10 ng/ml of IL-17A, IFNγ, or TNFα (all from PeproTech,

Hamburg, Germany), and various concentrations of prednisolone (MIBE GmbH Arzneimittel, Brehna, Germany). Chemokine levels in supernatants were determined after 24 h of incubation by using bead-based immunoassay technology.

Chemokine measurement. We used a bead-based immunoassay technology (LEGENDplex, BioLegend) to quantify the concentration of cytokines in supernatants of mouse kidney tubular cells. The premixed Mouse Proinflammatory Chemokine panel (catalog no. 740370) was applied to analyze the relevant chemokines by following the manufacturer's protocol. Values below the limit of detection were considered zero.

Assessment of the antigen-specific humoral immune response. Mouse anti-sheep IgG antibody titers were measured by ELISA using sera collected 10 days after induction of nephritis. In brief, ELISA microtiter plates were coated with 100 µl sheep IgG (100 µg/ml; Sigma, St Louis, MO) in carbonate–bicarbonate buffer overnight at 4 °C. After blocking with 1% bovine serum albumin in Tris-buffered saline (Sigma), plates were incubated with serial dilutions of mouse serum for 1 h at room temperature. Bound mouse IgG was detected using peroxidase-conjugated goat anti-mouse IgG (Biozol, Eching, Germany), TMB peroxidase substrate, and absorbance readings (450 nm). Lack of cross reactivity of the secondary antibody with sheep IgG was demonstrated by omitting the primary antibody. The bound mouse immunoglobulin isotypes were detected using peroxidase-conjugated rabbit anti-mouse IgG, IgG1, IgG2a/c, IgG2b, and IgG3 antibodies (Zymed-Invitrogen, Karlsruhe, Germany).

Statistics. The results are shown as the mean presented as a bar graph and superimposed single data points in a scatter dot plot. Differences between two individual experimental groups were compared using a two-tailed t test. In the case of three or more groups, a two-way ANOVA with Bonferroni's multiple comparisons test was used. Experiments that did not yield enough

independent data for statistical analysis because of the experimental setup were repeated at least three times. $P < 0.05$ was considered as statistically significant.

Study approval. All human studies were approved by the local ethics committee of the chamber of physicians in Hamburg (Ethik-Kommission der Ärztekammer Hamburg, registration numbers PV5026 and PV4806) and the Collaborative Research Centre (CRC) Board of the Hamburg Glomerulonephritis Registry (Central Service Project C1 of CRC1192). Written informed consent was obtained from all patients prior to their participation, and all studies were conducted in accordance with the ethical principles stated by the Declaration of Helsinki.

Author contributions

Conceptualization, J.H.R. and U.P.; acquisition, analysis, and interpretation of data, J.H.R., L.R., H.J.P., Y.Z., N.A., N.S., A.P., A.K., A.B., G.T., L.S., N.M.T., E.H., U.O.W., T.B.H., T.W., J.E.T., C.F.K., and U.P.; writing, J.H.R. and U.P.; visualization, J.H.R.; supervision, U.P. All authors approved the final version of the manuscript.

Acknowledgments

This work was supported by grants from the Deutsche Forschungsgemeinschaft (CRC 1192) to U.P. (A1 and C3), C.F.K. (A5 and C3), E.H. (C1), and T.W. (C1). The authors would like to thank Dr. Guido Hegasy for illustrating the graphical abstract. FACS sorting was performed at the FACS Sorting Core Unit of the University Medical Center Hamburg-Eppendorf.

References

1. Kurts C, et al. The immune system and kidney disease: basic concepts and clinical implications. *Nat Rev Immunol.* 2013;13(10):738-53.

2. Couser WG. Basic and translational concepts of immune-mediated glomerular diseases. *J Am Soc Nephrol.* 2012;23(3):381-99.

3. Krebs CF, et al. T helper type 17 cells in immune-mediated glomerular disease. *Nat Rev Nephrol.* 2017;13(10):647-59.

4. Suarez-Fueyo A, et al. T cells and autoimmune kidney disease. *Nat Rev Nephrol.* 2017;13(6):329-43.

5. Riedel JH, et al. T helper cell trafficking in autoimmune kidney diseases. *Cell Tissue Res.* 2021;385(2):281-92.

6. Kitching AR, and Hutton HL. The Players: Cells Involved in Glomerular Disease. *Clin J Am Soc Nephrol.* 2016;11(9):1664-74.

7. Chen A, et al. Bowman's capsule provides a protective niche for podocytes from cytotoxic CD8+ T cells. *J Clin Invest.* 2018;128(8):3413-24.

8. Taves MD, and Ashwell JD. Glucocorticoids in T cell development, differentiation and function. *Nat Rev Immunol.* 2021;21(4):233-43.

9. Ponticelli C, and Locatelli F. Glucocorticoids in the Treatment of Glomerular Diseases: Pitfalls and Pearls. *Clin J Am Soc Nephrol.* 2018;13(5):815-22.

10. Hardy RS, et al. Therapeutic glucocorticoids: mechanisms of actions in rheumatic diseases. *Nat Rev Rheumatol.* 2020;16(3):133-44.

11. Cain DW, and Cidlowski JA. Immune regulation by glucocorticoids. *Nat Rev Immunol.* 2017;17(4):233-47.

12. Tuckermann JP, et al. Macrophages and neutrophils are the targets for immune suppression by glucocorticoids in contact allergy. *J Clin Invest.* 2007;117(5):1381-90.

13. Klassen C, et al. Airway Epithelial Cells Are Crucial Targets of Glucocorticoids in a Mouse Model of Allergic Asthma. *J Immunol.* 2017;199(1):48-61.

14. Brix SR, et al. Development and validation of a renal risk score in ANCA-associated glomerulonephritis. *Kidney Int.* 2018;94(6):1177-88.

15. Panzer U, et al. Chemokine receptor CXCR3 mediates T cell recruitment and tissue injury in nephrotoxic nephritis in mice. *J Am Soc Nephrol.* 2007;18(7):2071-84.

16. Ohta K, and Yamashita N. Apoptosis of eosinophils and lymphocytes in allergic inflammation. *J Allergy Clin Immunol.* 1999;104(1):14-21.

17. Herold MJ, et al. Glucocorticoids in T cell apoptosis and function. *Cell Mol Life Sci.* 2006;63(1):60-72.

18. Steinmetz OM, et al. CXCR3 mediates renal Th1 and Th17 immune response in murine lupus nephritis. *J Immunol.* 2009;183(7):4693-704.

19. Paust HJ, et al. CXCR3+ Regulatory T Cells Control TH1 Responses in Crescentic GN. *J Am Soc Nephrol.* 2016;27(7):1933-42.

20. Rosenkranz AR, et al. P-selectin deficiency exacerbates experimental glomerulonephritis: a protective role for endothelial P-selectin in inflammation. *J Clin Invest.* 1999;103(5):649-59.

21. Heeringa P, et al. Lack of endothelial nitric oxide synthase aggravates murine accelerated anti-glomerular basement membrane glomerulonephritis. *Am J Pathol.* 2000;156(3):879-88.

22. van den Brandt J, et al. Enhanced glucocorticoid receptor signaling in T cells impacts thymocyte apoptosis and adaptive immune responses. *Am J Pathol.* 2007;170(3):1041-53.

23. Brewer JA, et al. Thymocyte apoptosis induced by T cell activation is mediated by glucocorticoids in vivo. *J Immunol.* 2002;169(4):1837-43.

24. Vacchio MS, and Ashwell JD. Glucocorticoids and thymocyte development. *Semin Immunol.* 2000;12(5):475-85.

25. Schweingruber N, et al. Chemokine-mediated redirection of T cells constitutes a critical mechanism of glucocorticoid therapy in autoimmune CNS responses. *Acta Neuropathol.* 2014;127(5):713-29.

26. Wust S, et al. Peripheral T cells are the therapeutic targets of glucocorticoids in experimental autoimmune encephalomyelitis. *J Immunol.* 2008;180(12):8434-43.

27. Inoue T, et al. Peritransplant glucocorticoids redistribute donor T cells to the bone marrow and prevent relapse after haploidentical SCT. *JCI Insight.* 2021;6(22):e153551.

28. Engler JB, et al. Glucocorticoid receptor in T cells mediates protection from autoimmunity in pregnancy. *Proc Natl Acad Sci U S A.* 2017;114(2):E181-E90.

29. Groom JR, and Luster AD. CXCR3 in T cell function. *Exp Cell Res.* 2011;317(5):620-31.

30. Karin N, et al. Biased signaling pathways via CXCR3 control the development and function of CD4+ T cell subsets. *J Leukoc Biol.* 2016;99(6):857-62.

31. Kuppe C, et al. Investigations of Glucocorticoid Action in GN. *J Am Soc Nephrol.* 2017;28(5):1408-20.

32. Li H, et al. IL-23 reshapes kidney resident cell metabolism and promotes local kidney inflammation. *J Clin Invest.* 2021;131(12):e142428.

33. Segerer S, et al. CXCR3 is involved in tubulointerstitial injury in human glomerulonephritis. *Am J Pathol.* 2004;164(2):635-49.

34. Enghard P, et al. CXCR3+CD4+ T cells are enriched in inflamed kidneys and urine and provide a new biomarker for acute nephritis flares in systemic lupus erythematosus patients. *Arthritis Rheum.* 2009;60(1):199-206.

35. Menke J, et al. CXCL9, but not CXCL10, promotes CXCR3-dependent immune-mediated kidney disease. *J Am Soc Nephrol.* 2008;19(6):1177-89.

36. Banchereau R, et al. Understanding Human Autoimmunity and Autoinflammation Through Transcriptomics. *Annu Rev Immunol.* 2017;35:337-70.

37. Bennett L, et al. Interferon and granulopoiesis signatures in systemic lupus erythematosus blood. *J Exp Med.* 2003;197(6):711-23.

38. Guiducci C, et al. TLR recognition of self nucleic acids hampers glucocorticoid activity in lupus. *Nature.* 2010;465(7300):937-41.

39. Szekanecz Z, et al. Autoinflammation and autoimmunity across rheumatic and musculoskeletal diseases. *Nat Rev Rheumatol.* 2021;17(10):585-95.

40. Sinha S, et al. Dexamethasone modulates immature neutrophils and interferon programming in severe COVID-19. *Nat Med.* 2022;28(1):201-11.

41. Riedel JH, et al. IL-17F Promotes Tissue Injury in Autoimmune Kidney Diseases. *J Am Soc Nephrol.* 2016;27(12):3666-77.

42. Krebs CF, et al. Pathogen-induced tissue-resident memory TH17 (TRM17) cells amplify autoimmune kidney disease. *Sci Immunol.* 2020;5(50).

43. Hao Y, et al. Integrated analysis of multimodal single-cell data. *Cell.* 2021;184(13):3573-87 e29.

44. Stuart T, et al. Comprehensive Integration of Single-Cell Data. *Cell.* 2019;177(7):1888-902 e21.

45. Wolf G, et al. Angiotensin II-induced hypertrophy of cultured murine proximal tubular cells is mediated by endogenous transforming growth factor-beta. *J Clin Invest.* 1993;92(3):1366-72.

Figures

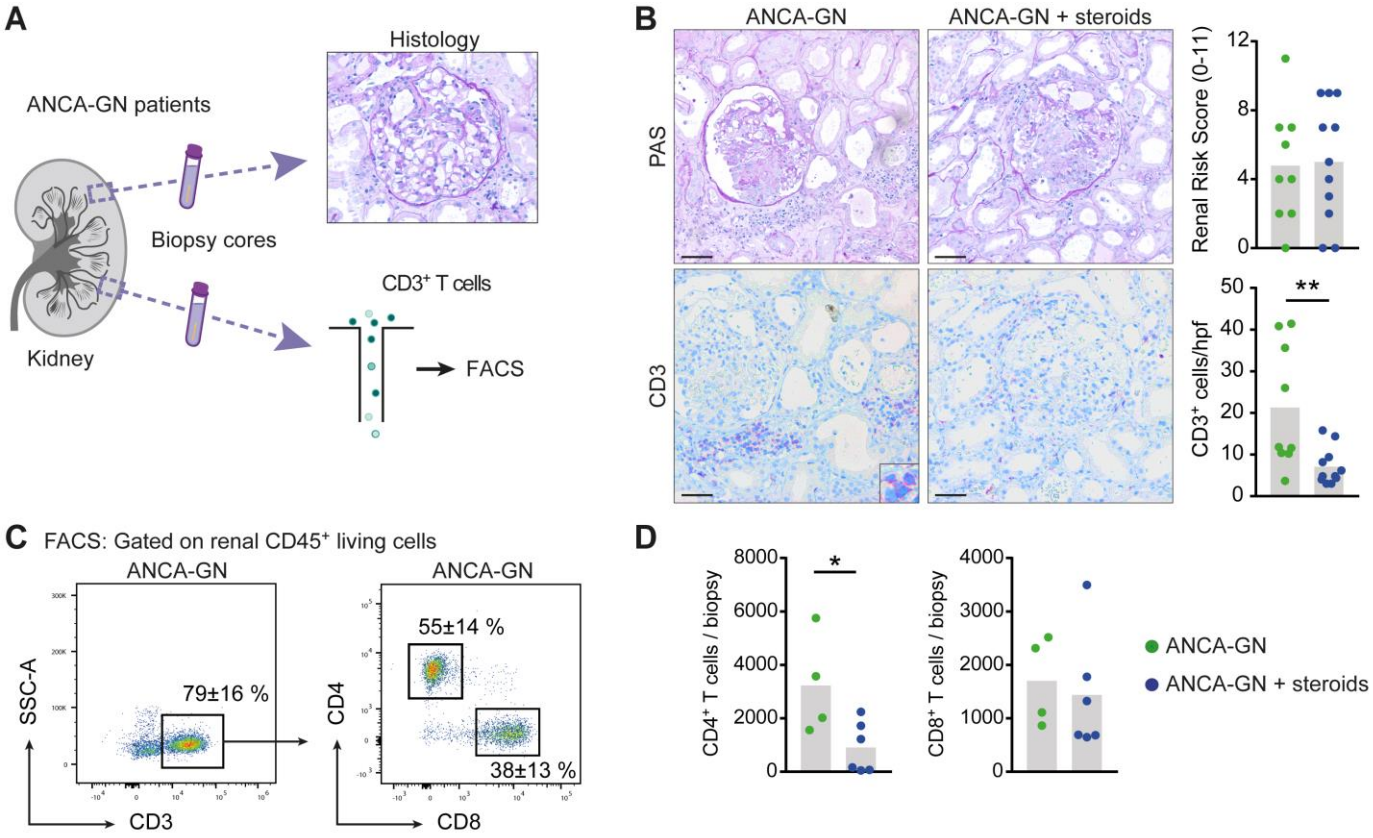

Figure 1. Glucocorticoid treatment rapidly reduces the renal CD4⁺ T-cell infiltrate in human ANCA-GN.

(**A**) Schematic representation of the experimental setup. (**B**) Representative photographs of Periodic Acid-Schiff (PAS)-stained kidney sections and the respective Renal Risk Score (14) of kidney biopsies obtained from untreated ANCA-GN patients and ANCA-GN patients after glucocorticoid treatment, as well as representative photographs of serial immunohistochemical CD3 staining and semiquantitative analysis of intrarenal T-cell numbers. (**C**) Representative flow cytometric plots showing mean percentages of $CD3^+$ cells of total $CD45^+$ cells and mean percentages of $CD3^+CD4^+$ and $CD3^+CD8^+$ T cells of total $CD3^+$ T cells in ANCA-GN patients. (**D**) Quantification of total renal $CD3^+CD4^+$ and $CD3^+CD8^+$ T cells of ANCA-GN patients with and without steroid treatment, scale bar: 25µm. Symbols represent individual data points, with the mean as a bar graph. Data were analyzed using a two-tailed t test. *$p < 0.05$, **$p < 0.01$.

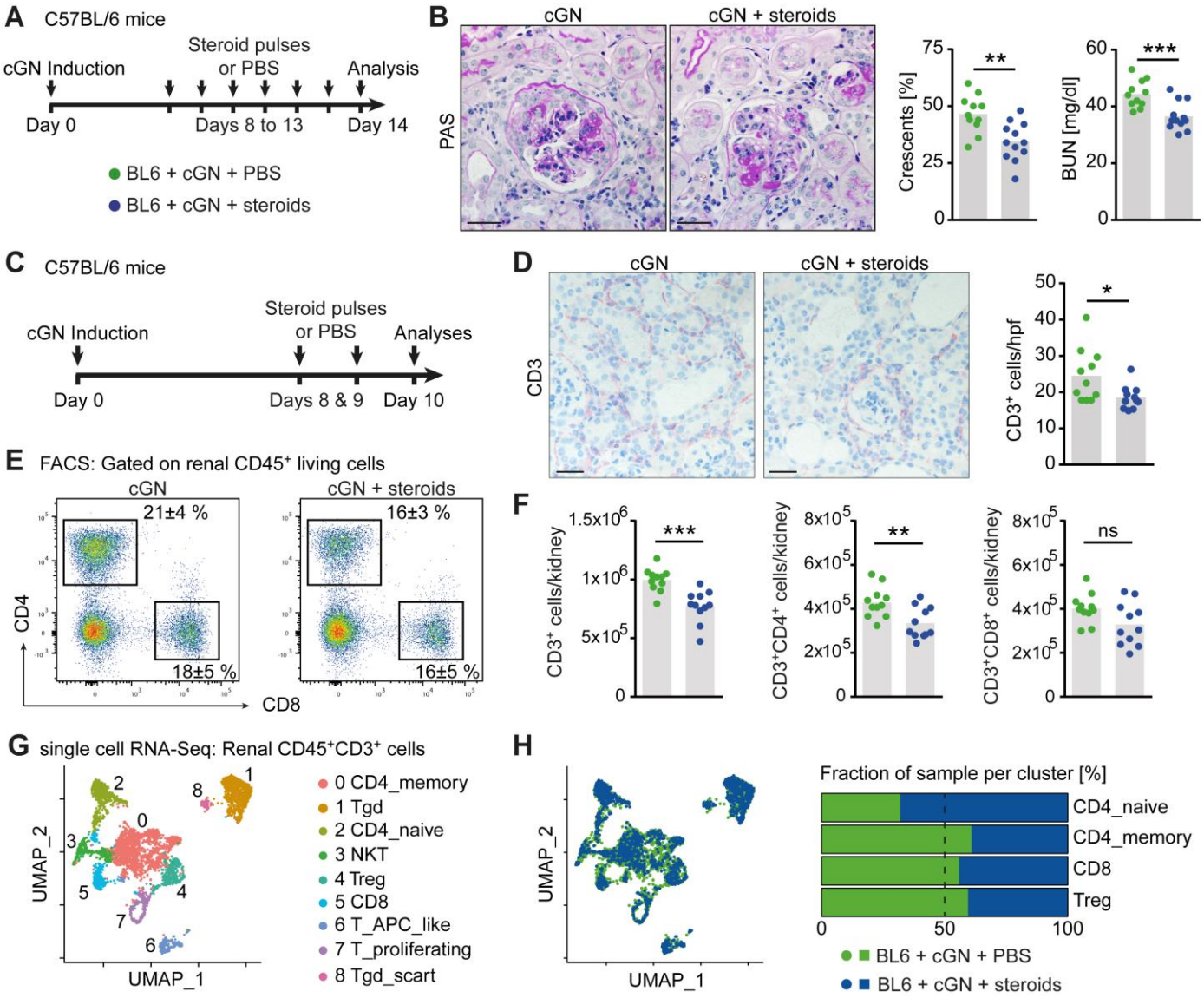

Figure 2. Glucocorticoids reduce the renal CD4⁺ T-cell infiltrate in murine cGN.
(**A**) Schematic representation of the experimental setup. (**B**) Representative photographs of PAS-stained kidney sections and quantification of crescent formation and BUN levels of untreated nephritic mice and mice treated for 6 consecutive days with high doses of steroids. (**C**) Schematic representation of the experimental setup. (**D**) Representative photographs of immunohistochemical CD3 staining of untreated and steroid-treated nephritic mice and semiquantitative analysis of intrarenal T cell numbers. (**E**) Representative plots showing mean percentages of renal $CD4^+$ and $CD8^+$ T cells and (**F**) quantification of flow cytometric analyses of changes in $CD3^+$, $CD3^+CD4^+$, and $CD3^+CD8^+$ T cells performed for the previously mentioned groups. (**G**) Uniform Manifold Approximation and Projection (UMAP) space of nine clusters defined by unsupervised clustering of single-cell RNA sequencing of renal $CD3^+$ T cells. (**H**) UMAP space generated by cell origin and proportion of samples contributing to four main T cell clusters in both groups mentioned before. Symbols represent individual data points, with the mean as a bar graph. Data were analyzed using a two-tailed t test. *p<0.05, **p < 0.01, ***p < 0.001, ns = not significant.

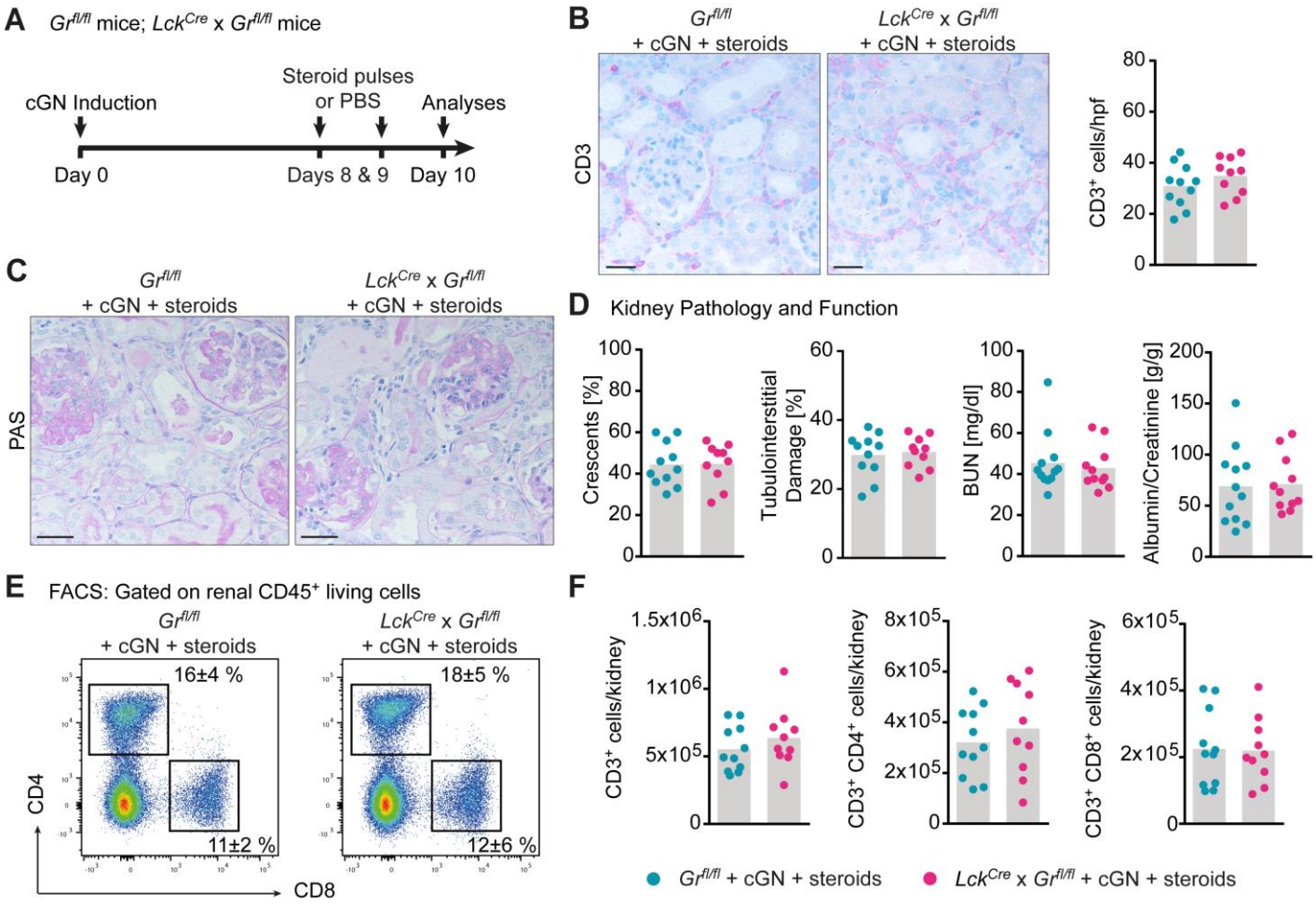

Figure 3. Glucocorticoid receptor (GR) deficiency in T cells does not prevent the reduction in renal CD4$^+$ T cells by glucocorticoids.

(**A**) Schematic representation of the experimental setup. (**B**) Representative photographs of immunohistochemical CD3 staining and semiquantitative analysis of intrarenal T-cell numbers of nephritic *Gr$^{fl/fl}$* and nephritic *Lck^{Cre}* x *Gr$^{fl/fl}$* mice with pulsed steroids. (**C**) Representative photographs of PAS-stained kidney sections obtained from the groups mentioned before. (**D**) Quantification of crescent formation, tubulointerstitial damage, BUN levels, and albumin/creatinine ratios determined for the previously mentioned groups. (**E**) Representative plots showing mean percentages of renal CD4$^+$ and CD8$^+$ T cells and (**F**) quantification of flow cytometric analyses of changes in CD3$^+$, CD3$^+$CD8$^+$, and CD3$^+$CD4$^+$ T cells performed for the groups mentioned before. Data are representative of three independent experiments. Symbols represent individual data points, with the mean as a bar graph. Data were analyzed using a two-tailed t test.

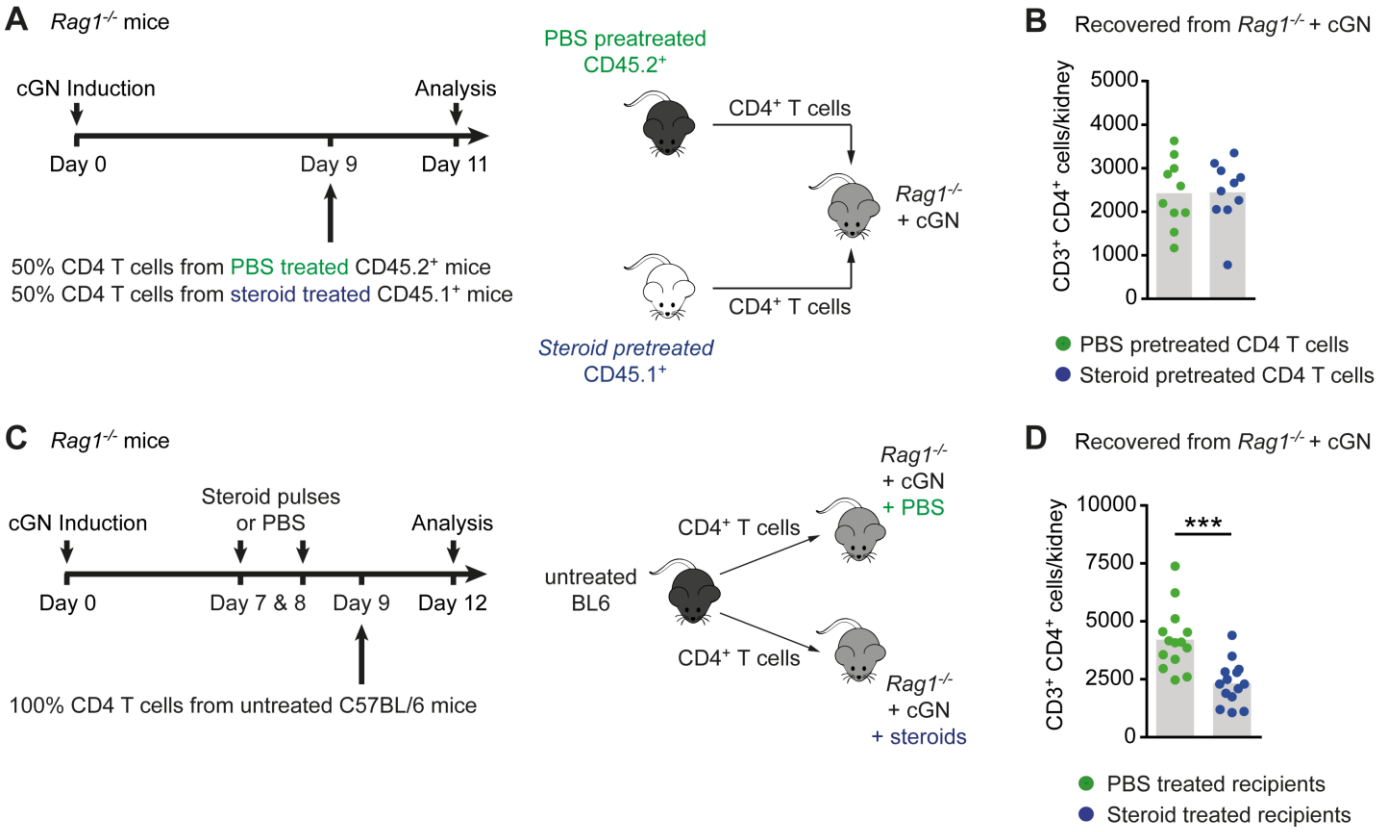

Figure 4. Glucocorticoid treatment changes the renal inflammatory environment to attenuate CD4$^+$ T-cell recruitment.

(**A**) Schematic representation of the experimental setup, and (**B**) numbers of recovered renal CD45.1$^+$ and CD45.2$^+$CD4$^+$ T cells from nephritic *Rag1*$^{-/-}$ mice after two days following intravenous transfer of a mixture of equal numbers of CD45.2$^+$CD3$^+$CD4$^+$ T cells from PBS- pretreated mice, and CD45.1$^+$CD3$^+$CD4$^+$ T cells from steroid-pretreated mice. (**C**) Schematic representation of the experimental setup, and (**D**) numbers of recovered renal CD4$^+$ T cells from PBS-treated and steroid-pulsed nephritic *Rag1*$^{-/-}$ mice after three days following intravenous transfer of CD3$^+$CD4$^+$ T cells into both groups. Symbols represent individual data points, with the mean as a bar graph. Data were analyzed using a two-tailed t test. ***$p < 0.001$.

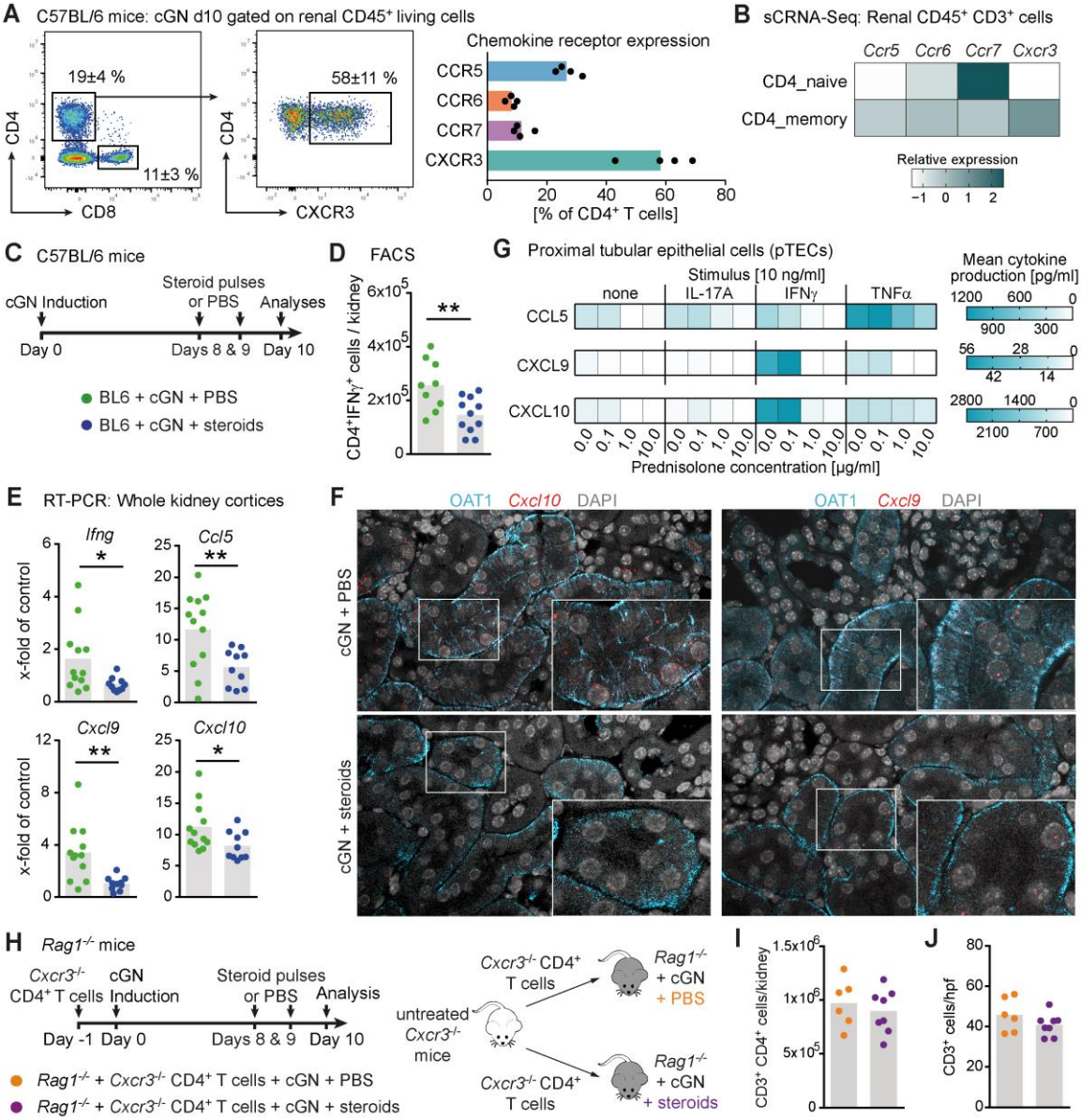

Figure 5. The recruitment of CXCR3$^+$ T$_H$1 cells in murine cGN is attenuated by glucocorticoids through the dampened production of the corresponding chemokines by tubular epithelial cells.

(**A**) Representative plots showing mean percentages of CD4$^+$ and CD8$^+$ T cells, respectively, and percentage CXCR3 positivity of CD4$^+$ T cells, as well as relative chemokine receptor expression of CD3$^+$CD4$^+$ T cells obtained from nephritic animals at day 10 of cGN determined by flow cytometric analyses. (**B**) Analysis of the single-cell RNA sequencing data of renal CD3$^+$ T cells of nephritic mice analyzed for relative chemokine receptor expression of the CD4_naive and CD4_memory clusters. (**C**) Schematic representation of the experimental setup, and (**D**) quantification of flow cytometric analyses of absolute numbers of CD3$^+$CD4$^+$IFNy$^+$ T cells isolated from kidneys of untreated and steroid-treated nephritic mice. (**E**) RT-PCR analyses of indicated mRNA expression from whole renal cortices of kidneys collected from the groups mentioned before. (**F**) RNA scope analyses show the preferential localization of *Cxcl9* and *Cxcl10* mRNA to the tubulointerstitial compartment and markedly reduced expression in steroid treated mice. (**G**) Heat map of chemokine protein levels in supernatants of proximal tubular epithelial cells after stimulation with either medium alone, IL-17A, IFNγ, or TNFα under increasing concentrations of prednisolone. (**H**) Schematic representation of the experimental setup, and (**I**) Numbers of recovered renal CD4$^+$ T cells from PBS-treated and steroid- pulsed nephritic Rag1$^{-/-}$ mice after eleven days following intravenous transfer of CXCR3^{neg} CD4$^+$ T cells into both groups. (**J**) Semiquantitative analysis of intrarenal T-cell numbers derived from kidney sections immunohistochemically stained for CD3 for the groups mentioned before. Symbols represent individual data points, with the mean as a bar graph. Data were analyzed using a two-tailed t test. *p<0.05, **p < 0.01.

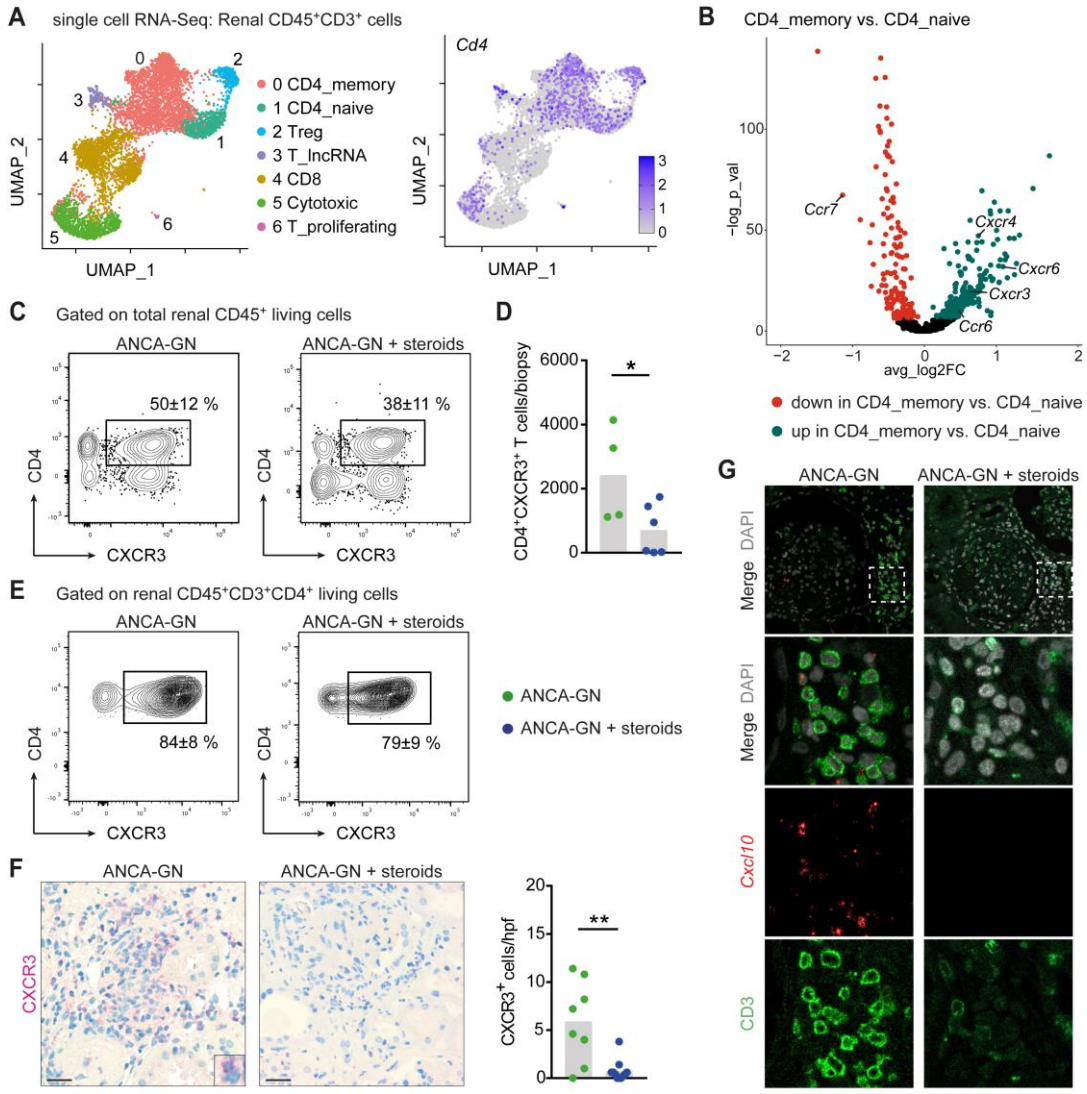

Figure 6. Glucocorticoid treatment alleviates the recruitment of CXCR3$^+$ TH1 cells to the kidneys of human ANCA-GN patients.

(**A**) Uniform Manifold Approximation and Projection (UMAP) space of seven clusters defined by unsupervised clustering of renal CD3$^+$ T cells from kidney biopsies of ANCA-GN patients treated with glucocorticoids and UMAP of *Cd4* expression in these clusters. (**B**) Volcano plot of differentially expressed chemokine receptor mRNA of the CD4_memory cluster compared to the CD4_naive cluster. (**C**) Representative flow cytometric plots showing mean percentages of CXCR3 positivity of renal CD45$^+$ cells in untreated ANCA-GN patients and ANCA-GN patients after glucocorticoid treatment and (**D**) quantification of total renal CD3$^+$CD4$^+$CXCR3$^+$ T cells in these groups. (**E**) Representative flow cytometric plots showing mean percentages of CXCR3 positivity of renal CD3$^+$CD4$^+$ T cells in untreated ANCA-GN patients and ANCA-GN patients after glucocorticoid treatment. (**F**) Representative photographs of CXCR3 stained kidney sections from kidney biopsies of untreated ANCA-GN patients and ANCA-GN patients after glucocorticoid treatment and semiquantitative analysis of intrarenal CXCR3 positive cells in these groups. (**G**) Combination of immunofluorescence staining of CD3 with *Cxcl10* RNAscope analysis of kidney sections from kidney biopsies of untreated ANCA-GN patients and ANCA-GN patients after glucocorticoid treatment. Symbols represent individual data points, with the mean as a bar graph. Scale bar: 25µm. Data were analyzed using a two-tailed t test. *$p < 0.05$, **$p<0.01$.